END-TO-END CONTROL SYSTEM VERIFICATION
OF THE STARLAB EXPERIMENT

Dr Dan Herrick
Dr Jack Rodden
Capt Paul Shirley

19980309 295

DTIC QUALITY INSPECTED 4

Accession Number: 3747

Publication Date: Feb 03, 1990

Title: End-to-End Control System Verification of the Starlab Experiment (Paper)

Personal Author: Herrick, D.; Rodden, J.; Shirley, P.

Corporate Author Or Publisher: American Astronautical Society, P.O. Box 28130, San Diego, CA 92128 Report Number: AAS 90-045

Comments on Document: Paper given at the Annual Rocky Mountain Guidance and Control Conference, Keystone, CO: February 3-7, 1990

Descriptors, Keywords: STARLAB Experiment Electro-Optics Beam Control Acquisition Tracking Pointing ATP

Pages: 14

Cataloged Date: Sep 23, 1992

Document Type: HC

Number of Copies In Library: 000001

Record ID: 24783

END-TO-END CONTROL SYSTEM VERIFICATION OF THE STARLAB EXPERIMENT*

Dr Dan Herrick**
Dr Jack Rodden†
Captain Paul Shirley‡

This paper describes an electro-optical tracking and beam control system simulation used to analyze the performance for the space shuttle based STARLAB experiment hardware. STARLAB is to provide an on orbit demonstration of acquisition, tracking and pointing (ATP) techniques critical to strategic defense directed energy concepts. In particular, a target booster will be optically tracked from launch to re-entry. This rocket will be instrumented to "score" how accurately a laser beam can be pointed by the experiment. This paper focuses on techniques used to predict on-orbit performance based on laboratory testing and simulations.

A comprehensive end-to-end simulation of the STARLAB hardware/software has been constructed. The simulation includes detailed models of the optical tracker, including target imagery; the beam control servos and structural dynamics. Detailed sensor noise and line of sight disturbance models are included. In addition, actual flight software is integrated into the simulation to allow functional checkout of its algorithms. Simulation modules are developed in a user friendly workstation environment with easily accessible time and frequency domain analysis tools that permit rapid model verification. Comprehensive, end-to-end time domain simulations are executed using code generation features of the simulation environment which permit execution of the simulation on supercomputers. This simulation has been used to validate the experiment design and can be used to support laboratory hardware integration, mission planning, training, mission operations and post flight data analysis.

THE STARLAB MISSION

The STARLAB mission, planned for launch in late 1991, will be used to conduct acquisition, tracking and pointing (ATP) experiments from the space shuttle platform. The purpose of these experiments is to resolve critical technology issues associated with the development of space based defenses against strategic ballistic missiles. Technology issues associated with both directed and kinetic energy weapons will be addressed with an emphasis on directed energy applications.

The principle ATP requirements for a spaceborne directed energy weapon are to measure a target's position accurately with respect to its highly stabilized line of sight and to point its high energy beam at a vulnerable aimpoint on the target. The technology issues raised by these requirements that will be addressed by STARLAB include:

Detection and optical tracking of a booster using passive plume radiation.

Location of the booster body using information derived from the plume.

Actively tracking the booster body with an illumination laser.

Precise stabilization and pointing of a low power scoring laser at a specific aimpoint on the booster.

Using plume light to correct for optical distortions in the beam train in order to increase laser intensity at the aimpoint.

Plume characteristics for both solid and liquid boosters.

Multi-spectral, high resolution earth and space background characteristics.

During a 7 day mission, STARLAB will engage a test booster called STARBIRD that is equipped with a laser scoreboard to demonstrate the ATP functions described above. The STARBIRD experiment is depicted in Figure 1. The shuttle will be flown in a 330 km orbit inclined at 33 degrees. The STARLAB payload configuration includes the Spacelab double module and a pallet as is shown in Figure 2. The external pallet carries an 80 centimeter beam expander. The shuttle attitude is controlled to keep targets within the field of regard of a gimbaled pointing flat positioned in front of the beam expander. Visible acquisition, infrared and ultraviolet optical imagers are located on the pallet along with the active track laser illuminator. The optical line of sight is carried into the manned module

where the wavefront control adaptive optics, aimpoint tracker focal planes and low power scoring laser are located.

TRACKING AND BEAM CONTROL SYSTEM

A conceptual view of the STARLAB pointing and tracking control system is shown in Figure 3. A hierarchy of control loops are required to perform the mission. At the bottom level are stabilization loops which attempt to optically couple the pallet and module benches and reject line of sight jitter caused by shuttle base motion. The alignment diode assembly (ADA) injects a beam that goes through the telescope and past the fast steering mirror to an angle sensor called the pallet vibration sensor (PVS). The fast steering mirror (FSM) stabilizes this alignment beam on the PVS. The ADA is located near a gyro/inertial angle sensor whose output is fed forward to the FSM loop to effectively stabilize the line of sight with respect to inertial space. The beam walk mirrors are driven to maintain alignment between the two optical benches. The net effect of these loops is to inertially stabilize the optical line of sight from the telescope to the tracking focal planes. The line of sight of the instrument is slewed by a large gimbaled pointing flat that is rate stabilized. Any residual pointing mirror jitter sensed by the rate loop gyro/IAS is fed to the fast steering mirror for rejection. Since the pallet vibration sensor has a very limited angular field of view, its offset from null is fed to the gimbal rate loop to avoid driving the ADA beam off the PVS. The net effect of the rate loop and rate gyro feed forward is to inertially stabilize the line of sight to output space. The track loop is closed on either a 60 Hz "coarse" track focal plane which views the booster plume or a 20 Hertz "fine" track focal plane which views reflected return of an illuminator laser. The track loop is wrapped around the rate loop described above. The marker or scoring laser beam, which is boresighted to the tracker focal planes, is commanded with track and point ahead errors so that it will hit the target. The illuminator laser is similarly pointed at the target. Tracker control loop compensation is shown in the single axis idealization of Figure 4. Although the beam walk mirror system sits in the tracker line of sight, it has no impact on the dynamics of the track loop. The coupled pointing/fast steering mirror plant looks effectively like a P/I compensator. To follow accelerating targets another integrator is introduced into the track loop. Estimated target rates are input to the mirror rate command point to further reduce the tracker servo hangoff. The approach to coupling the fast steering and pointing mirrors to form a "P/I" plant is shown in Figure 4. As discussed above, the significant features of the coupling between the fast steering and pointing mirrors are the FSM offload which keeps the ADA alignment beam within the PVS field of view; the gyro error fed to the FSM to reduce line of sight jitter caused by the pointing mirror gimbal; the track error fed to both the pointing mirror and the FSM to create desirable combined plant dynamics.

3

As can be seen, the optical line of sight of such an instrument is transformed by telescopes and gimbaled mirrors. This will make a target image on the tracker focal plane rotate as a function of gimbal angles. The control system must take these transformations into account when feeding back rate and tracking errors. The optical path from the pointing flat to the focal plane assembly passes some 26 optical surfaces. Figure 5 identifies groupings of optical surfaces used for the derived transformations. Each group of mirrors can be represented by a 3x3 transformation matrix relating an output optical ray to an input vector. These grouped optical transformations are interleaved by transformations related to the moveable surfaces. The mathematical representation of line of sight to the detector, $\underline{FPA}$, as a function of the line of sight vector, $\underline{T}$, is then:

$$\underline{FPA} = [A_g + B_g(\Theta_F) + D_g(\Psi_U) + F_g(\Psi_V) + C_g(\Psi_F) + E_g(\Theta_U) + G_g(\Theta_V)][G]^{-1}[P][G]\underline{T}$$

where:

$$A_g = [H3][BW2][BW1][H2][FSM][H1]$$
$$B_g = [H3][BW2][BW1][H2][\text{Perturbed } FSM_x][H1]$$
$$C_g = [H3][BW2][BW1][H2][\text{Perturbed } FSM_y][H1]$$
$$D_g = [H3][BW2][\text{Perturbed } BW1_x][H2][FSM][H1]$$
$$E_g = [H3][BW2][\text{Perturbed } BW1_y][H2][FSM][H1]$$
$$F_g = [H3][\text{Perturbed } BW2_x][BW1][H2][FSM][H1]$$
$$G_g = [H3][\text{Perturbed } BW2_y][BW1][H2][FSM][H1$$

$$[G] = \begin{bmatrix} c(\Theta_b) & 0 & -s(\Theta_b) \\ 0 & 1 & 0 \\ s(\Theta_b) & 0 & c(\Theta_b) \end{bmatrix}$$

$$[P] = \begin{bmatrix} 1-2c^2(\Theta)c^2(\Psi) & -2c^2(\Theta)c(\Psi)s(\Psi) & 2c(\Theta)s(\Theta)c(\Psi) \\ -2c^2(\Theta)c(\Psi)s(\Psi) & 1-2c^2(\Theta)s^2(\Psi) & 2c(\Theta)s(\Theta)s(\Psi) \\ 2c(\Theta)s(\Theta)c(\Psi) & 2c(\Theta)s(\Theta)s(\Psi) & 1-2s^2(\Theta) \end{bmatrix}$$

Where Θ_0 is the fixed pitch of gimbal azimuth axis, Θ is the inner gimbal elevation axis and Ψ is the outer gimbal azimuth axis. The transformation between the Target Vector, T, and the input ray FPA, to the detector involves the reflection transformation across the pointing mirror, P, transformed to vehicle coordinates which is a function of the variable gimbal angles. The fixed transformation A_g is the relation between the mirror reflection ray and the FPA input vector. The other matrices B_g, D_g .. G_g are the perturbations of the total transformation proportional to small rotations of the moveable surfaces of the fast steering and beam walk mirrors. The end-to-end transformation gives the relation between target and detector 3 dimensional vectors in vehicle coordinates. The required controller transformations are shown in the block diagram in Figure 6. The transformations relating detector signals to gimbal, gimbal to FSM, and FSM to gimbal are functions of gimbal angular positions. The elements of these matrices, along with the one relating bench motion rates to gimbal rates are updated by the flight computer at 60 Hz.

STARLAB PERFORMANCE SIMULATION

The performance of this control system is measured in terms of marker beam positioning with respect to the target. Beam jitter and offset from the desired aimpoint must be minimized. The primary sources of jitter are sensor noise and unrejected line of sight disturbances caused by base motion and atmospheric refraction within the manned module. The STARLAB tracking and pointing control system has been modeled with a computer simulation. The primary purpose of this simulation has been to predict marker beam jitter and tracker performance. In addition, this model serves as a guide to laboratory testing. Validating all component assumptions in the model with lab measurements increases confidence that the actual hardware will work as anticipated. This simulation will also be used during the STARLAB mission to predict the performance of the STARBIRD encounter from data collected on prerequisite on-orbit experiments such as tracker observations of stars and space targets carrying corner reflectors.

A commercial simulation program called MATRIX-X was used to model the STARLAB control system. The simulation contains a number of distinct types of models. At its core it contains a continuous system description of the mirror control loops. The gyro, optical alignment and inertial feed forward loops are described by continuous frequency domain transfer functions. Line of sight dynamics are generated by target and shuttle trajectory models. Line of sight jitter disturbances and sensor noises are input to the simulation in terms of power spectral densities. The rest of the control system is modeled in discrete time blocks. Track sensor noise is produced by a model of the actual imaging process.‡ The target imagery, both passive plumes and active target board signatures, are generated on a frame by frame basis. Images are radiometrically scaled, spatially blurred with the system's optical transfer function and sampled by the focal plane. Noise is added to each sampled pixel of the image. Track processor centroiding algorithms and mode logic are simulated. Flight software algorithms in the controller's digital processors are also included in the simulation. The actual C-code used in these processors was adapted to the simulation. Flight code segments that interface to the flight hardware and operating system are replaced with appropriate code to interface to the simulated flight hardware signals. Algorithmic flight code was left essentially intact.

This simulation can be used to examine details of the tracking process. Figure 7 shows representative plume and target board images which are processed by the tracker. Figure 8 shows are example of transition from "coarse" plume tracking to "fine" target board tracking. The track box is the highlighted square that overlays the tracked object in Figure 9. Only the data in the track box are processed to obtain track errors. This greatly reduces processing and suppresses noise. In the case shown here, the transition to fine track is smooth. The initial track box size and processing threshold were adjusted to their desired steady state values for this target. Poor selection of these parameters could have upset the transition. These interactions are important to understand because they may consume a considerable amount of the engagement timeline and they may result in failures to achieve some modes of operation.

The simulation is hosted on Sun and VAX workstations. These offer excellent interactive platforms for checking out the model at the component and subsystem level. The entire model, however, is quite computationally intensive. To achieve reasonable simulation turn around times, the MATRIX-X Hypercode feature is used. This reduces the servo model to a FORTRAN code that can be run on any machine with appropriate FORTRAN and C compilers. In the case of STARLAB, the simulation is run

---

‡ Image tracker model originally programmed by Scientific Simulations, Incorporated, under subcontract to RDA.

6

on a CRAY-II computer at the National Test Facility (NTF) at Falcon Air Force Base, Colorado. By using the MATRIX-X hypercode feature and the CRAY-II computer a 50 fold increase in simulation execution rates are realized. Off site communication between the MATRIX-X workstation and the NTF CRAY-II will be via a 1.5 megabit/sec T1 link.

TEST DATA FOR MODEL VALIDATION

The STARLAB hardware will be integrated and tested on the ground. Figure 9 shows the flight pallet and module benches as well as an autocollimator used to present target imagery to and accept the marker beam from the flight experiment. The principle shortcomings of this test environment are:

Structures and large optics are gravity loaded rather than weightless.

Tracking is done with the pointing mirror nearly static rather than slewing as in actual encounters.

The entire beam train is exposed to the atmosphere.

Base motion is not matched to that expected on the space shuttle.

Target phenomenology cannot be reproduced to represent space experiment encounters.

It is believed that in this end-to-end test setup, and subsystem testing leading up to this point, the beam control system can be sufficiently characterized to reduce performance uncertainty to that related to detailed shuttle base motion and target radiometric characteristics. To accomplish this, laboratory tests should adequately characterize all servo transmission characteristics, self generated base motion disturbances and sensor noise characteristics.

Coherence analysis techniques will be used to estimate the power spectra of sensor noise and line of sight disturbances. These techniques can be usefully employed in cases where sensors are measuring the same or linearly correlated physical quantities. The lack of coherence between the measurements provides clues about sensor noise characteristics. In the most straight forward case, where identical sensors are setup to measure the same physical signal, there should be the least ambiguity in interpreting the results. This approach is illustrated in Figure 10. For example, the two gyro/inertial angle sensor packages can be placed on the same base. This base can be excited with broadband forces to levels of expected on-orbit motion. The incoherent measurement spectra of these instruments provides an good estimate of the basic instrument noise. An alternative to this kind of test is to establish an exquisitely quiet seismic environment and measure

the sensor noise spectrum directly. At the levels that the STARLAB beam control system is expected to operate, this is difficult. The coherence analysis proposed here is susceptible to correlated sensor noise sources. The possibility of being fooled by correlated noise is reduced by system level tests that examine the correlated outputs of dissimilar sensors. Figure 11 illustrates a system level test of the inertial feedforward beam stabilization subsystem. Here a high signal to noise ratio track source is used. This reduces tracker noise to a minimum. The target is viewed by two optical sensors. Motion of the three optical benches is measured by inertial sensors. A multiple and partial coherence analysis is performed between the base motion and the tracker signals. The part of the tracker signal that is coherent with the base motion is related to unrejected base motion while the incoherent part is related to tracker and other sensor noise. Marker beam jitter can also be measured in the target set to confirm the accuracy of the coherence-based estimate. Such an experiment offers a wealth of data for characterizing the performance of the beam control system.

The coherence test and analysis techniques will focus on quantifying cause/effect relationships that determine STARLAB beam control performance. Sensor noise, which is a principle determinant of beam control performance, should be well characterized prior to flight even in a relatively disturbance rich laboratory environment. While shuttle base motion for the STARLAB configuration is not well characterized, the performance characteristics of the inertial feedforward subsystem will be well characterized. An on-orbit characterization of the inertial feedforward subsystem will be performed using a high signal to noise ratio track source much like the lab test described above. By thoroughly characterizing the beam control system in lab tests it will be much easier to interpret the systems response to actual on-orbit target signatures and base motion.

CONCLUSIONS

The STARLAB experiment is designed to demonstrate impressive levels of target tracking and laser beam stabilization in a space environment. In order to successfully integrate and test this hardware, detailed simulations and sophisticated data analysis is mandatory. This paper described STARLAB experiment, associated performance simulations and the use of lab test results to ground critical noise and disturbance assumptions in those simulations.

REFERENCES

Van Allen, R. L., Dillow, J. D., Gurski, G. F., "Directed Energy Weapons Tracking and Pointing Space Experiments", AAS 87-031, presented at the 10th Annual Guidance and Control Conference, January 31-February 4, 1987, Keystone CO.

Rodden, J. J., "Mirror Line of Sight on a Moving Base", AAS 89-030, presented at the 12th Annual AAS Guidance and Control Conference, February 4-8 1989, Keystone CO.

Rodden, J. J., "Multimirror Beam Control", SPIE 1111-30, presented at The International Society for Optical Engineering 1989 Technical Symposia on Aerospace Sensing, 27-31 March 1989, Orlando, Florida.

Bendat, J. S. and Piersol, A. G., Engineering Applications of Correlation and Spectral Analysis, J. Wiley & Sons, 1980. Smith, W. J., "Modern Optical Engineering", McGraw-Hill Book Co., 1966.
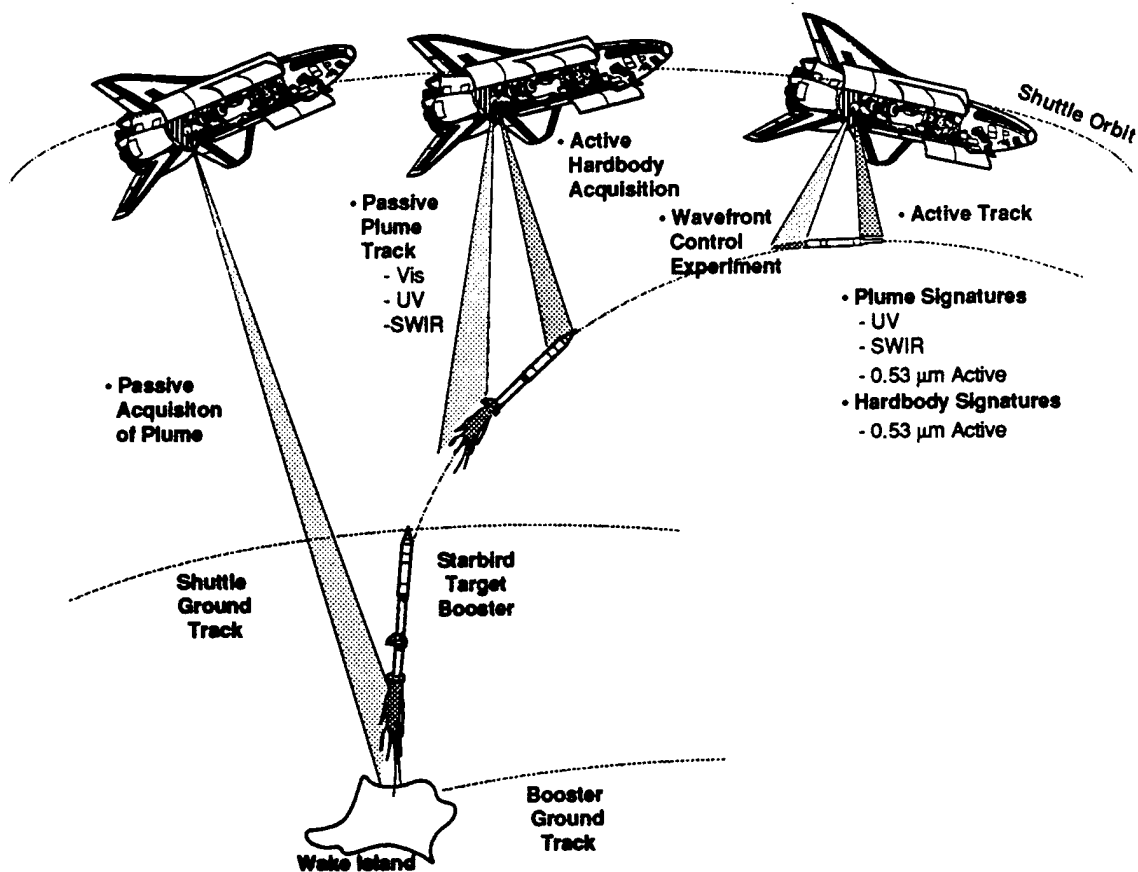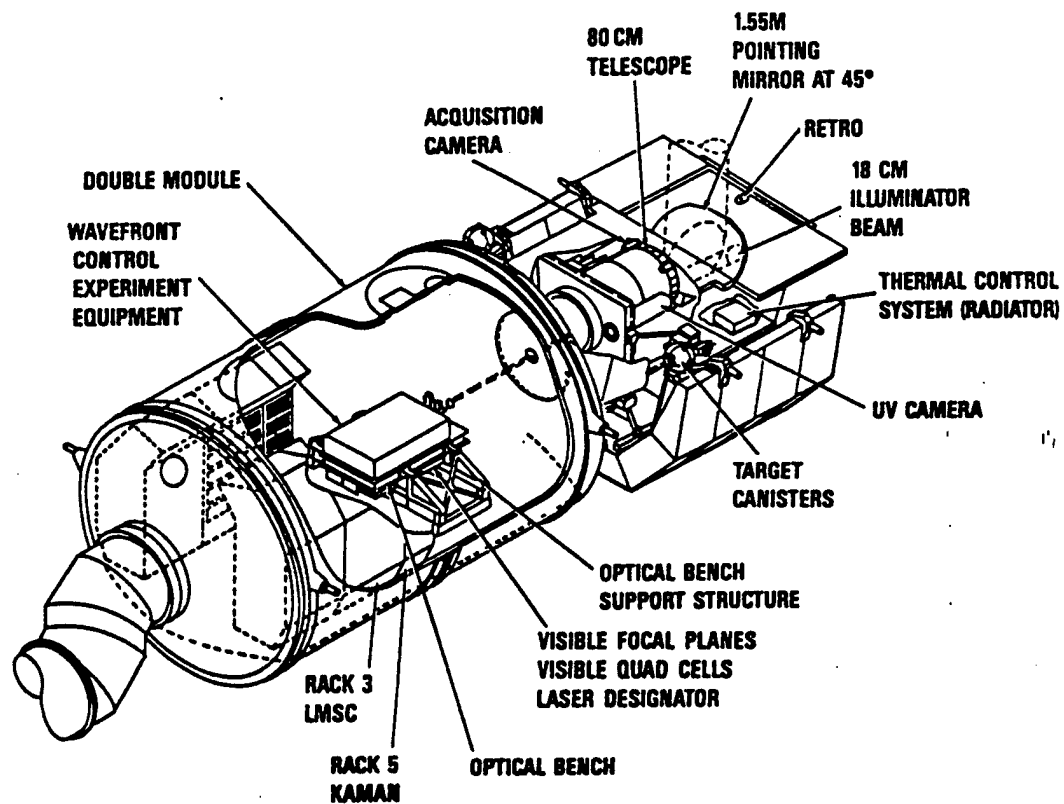
Figure 1. STARBIRD Engagement
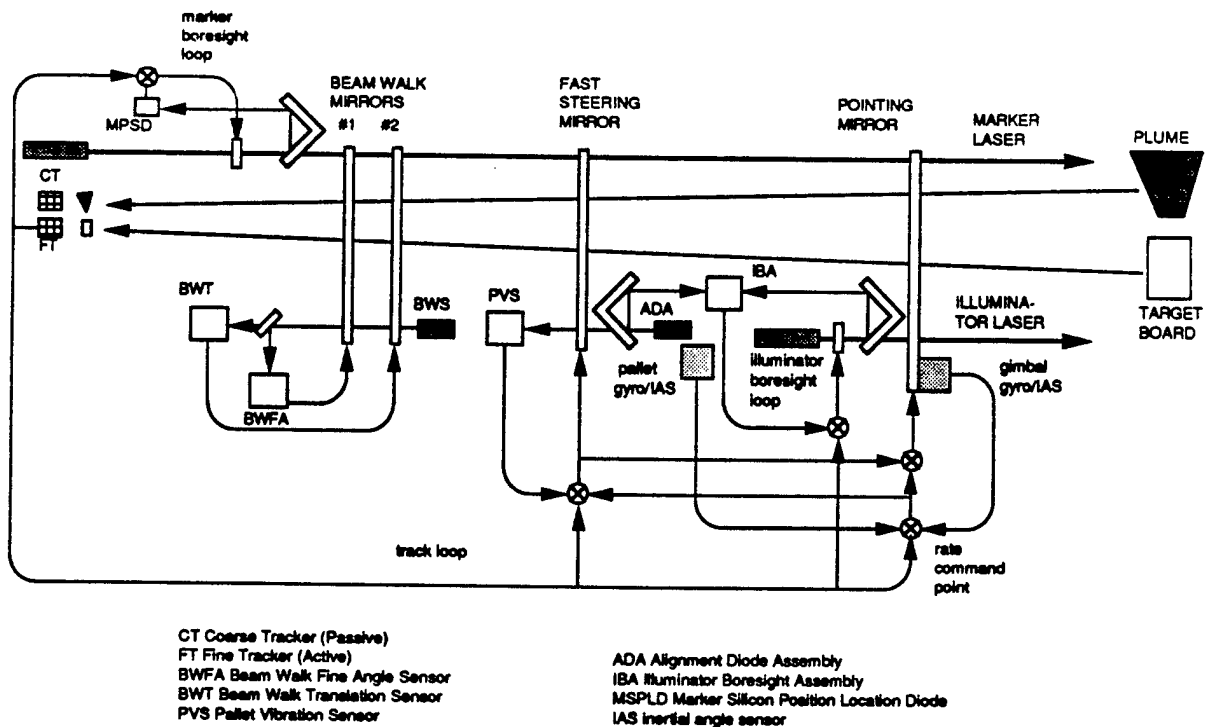
Figure 2. Experiment Payload Configuration

CT Coarse Tracker (Passive)
FT Fine Tracker (Active)
BWFA Beam Walk Fine Angle Sensor
BWT Beam Walk Translation Sensor
PVS Pallet Vibration Sensor

ADA Alignment Diode Assembly
IBA Illuminator Boresight Assembly
MSPLD Marker Silicon Position Location Diode
IAS Inertial angle sensor

Figure 3. Beam Control Concept

10

Pallet Base
Motion

Reference Rate & Pallet
Inertial Feed Forward

Gryo

Pointing
Mirror Rate

Gimbal Rate Servo Loop

Target
Los

Tracker

$C_3 + \dfrac{I_3}{S}$

Structural
Mode
Filter

$\dfrac{1/J}{S}$

$\dfrac{1}{S}$

Instrument
Los

$\dfrac{m}{S}$

FSM Offload

$K_4 + I_4/S$

mK_t

$K_F + \dfrac{K_1}{S}$

Fast Steering
Mirror

$\dfrac{1}{m}$

Sensor

Equivalent Transfer Function

Target
Los

Tracker

$C_3 + \dfrac{I_3}{S}$

$\dfrac{2(1 + K_t S)}{S}$
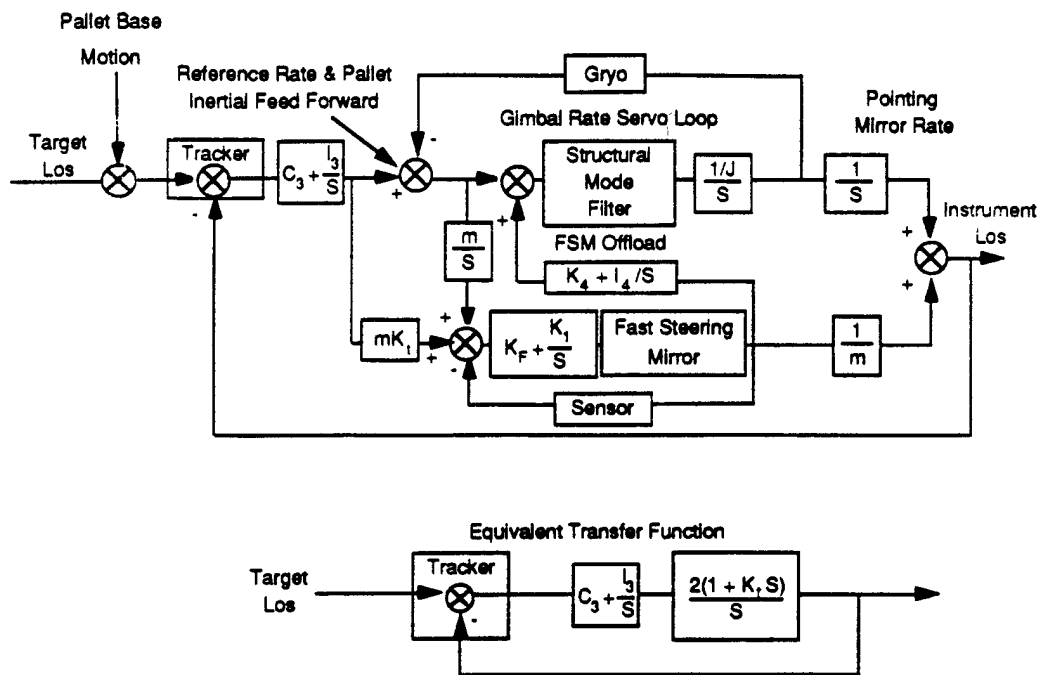
Figure 4. Conceptual Controls Block Diagram

Telescope

800mm
Entrance
Pupil

PM

F1

F2

FSM

Pupil Image 1

OAPM 3

FPA Detectors

SWAT
FILTER

50
mm

FPA
Entrance

FPA
Fold

Pupil
Image
3

Corner
Cube

OAPM 1

IRBS

F5

60mm

BW 1

Marker
Mirror

SPACELAB
WINDOW

Marker
Laser

18.5
mm

F4

BW 2

OAPM 2

F3

BWBS

MM 3

OAPM 4

RWG BS

Pupil Image 2
w/o WCE

OAPM 5

Wave Front
Control
Experiment

F 6

BP 2

F8 F9

Deformable
Mirror

Exit
BS

BP 1

MM 4

Pupil image 2
w WCE

F 7

BP 3

BP 4

P

H1

H2

H3

PM

Telescope+F1+
OAPM1 + F2

FSM

OAPM2+F3+F4+
F5+OAPM3

BW1

BW2

BP1+BP2+BP3+BP4+
OAPM4+F8+F9+OAPM5

Figure 5. Optical Path

11

Figure 6. Mirror Control Distribution

Fine Tracking Target Board Image   Coarse Tracking Plume Image
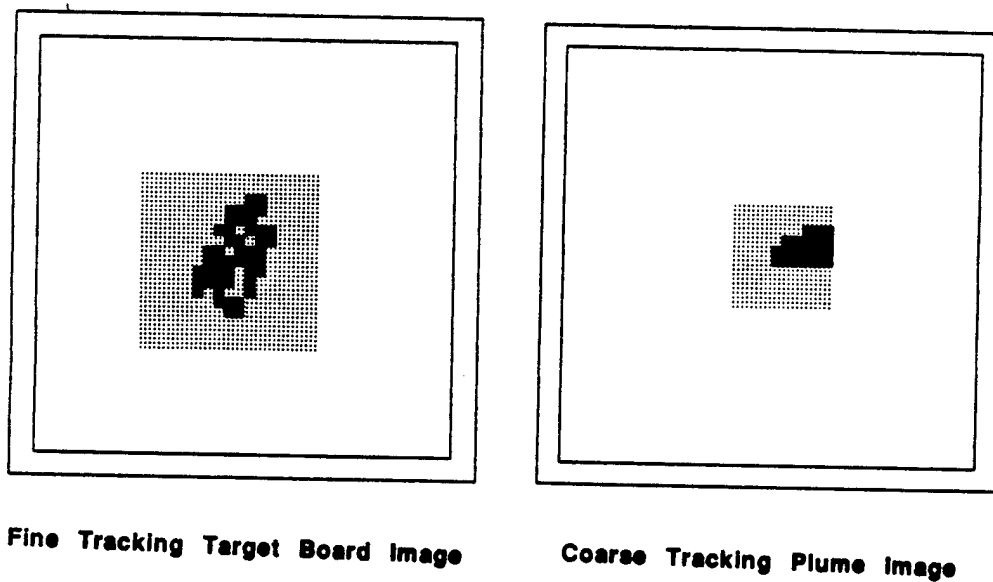
Figure 7. Simulated STARBIRD Imagery

12
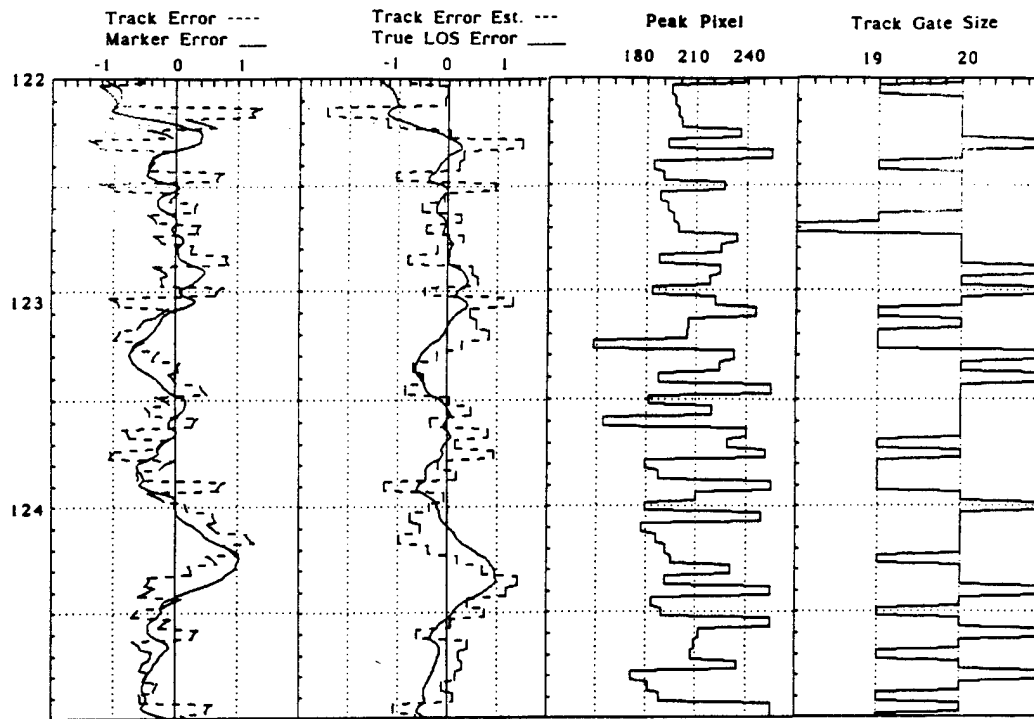
Figure 8. Simulated Fine Track Transition
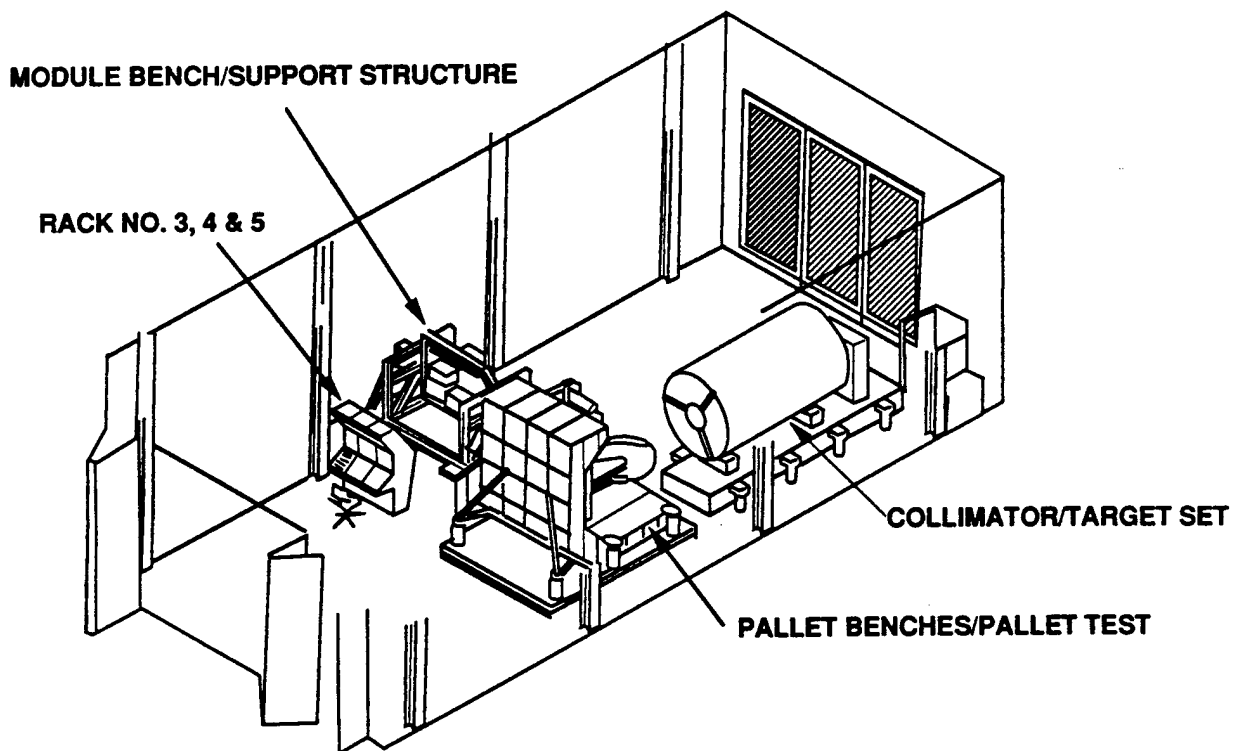
Figure 9. Integration and Test Lab Setup

$$N_x(t)$$

$$Z(t)$$

$$H_x(f)$$

$$x(t)$$

$$H_y(f)$$

$$y(t)$$

$$N_y(t)$$
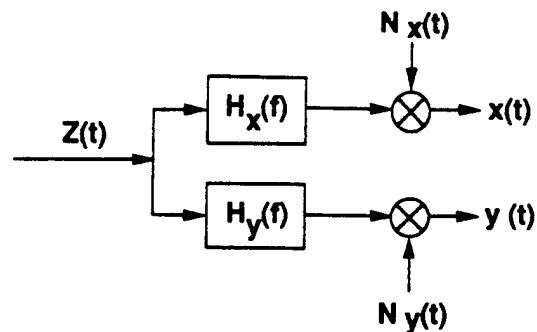
$$G_{n_x n_x}(f) = [1 - \gamma_{xy}^2] G_{xx}(f)$$

$$G_{n_y n_y}(f) = [1 - \gamma_{xy}^2] G_{yy}(f)$$

$$G_{xx}$$

$$(1 - \gamma_{xy}^2)$$

$$1.0$$

$$G_{n_x n_x}$$

$$X$$

$$=$$

$$f$$

$$f$$

$$f$$
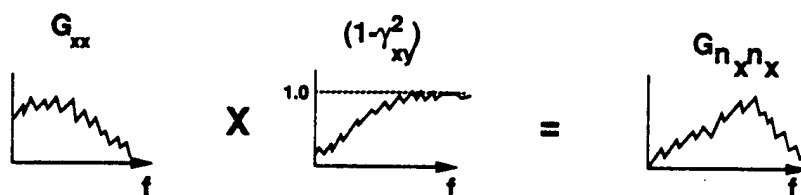
Figure 10. Parallel Sensor Characterization

beam
motion
mirror

MODULE BENCH   PALLET BENCH   TARGET BENCH

RQUAD

target beam source

WAVE   FSM

MARKER   WCE   ISA   PM   IAS or   MARKER
                                          MHD   SCORING

Inertial Instruments

RQUAD Measurement

RQUAD w/ WAVE conditioned out

RQUAD w/ WAVE & ISA conditioned out

RQUAD w/ WAVE, ISA & IAS conditioned out
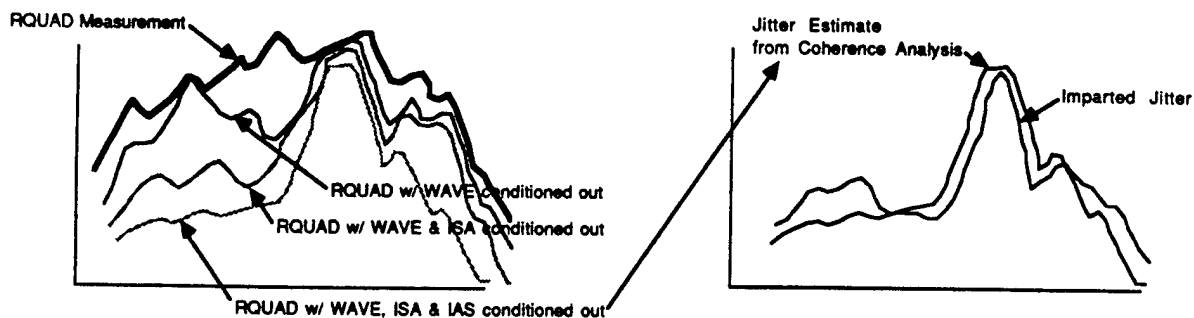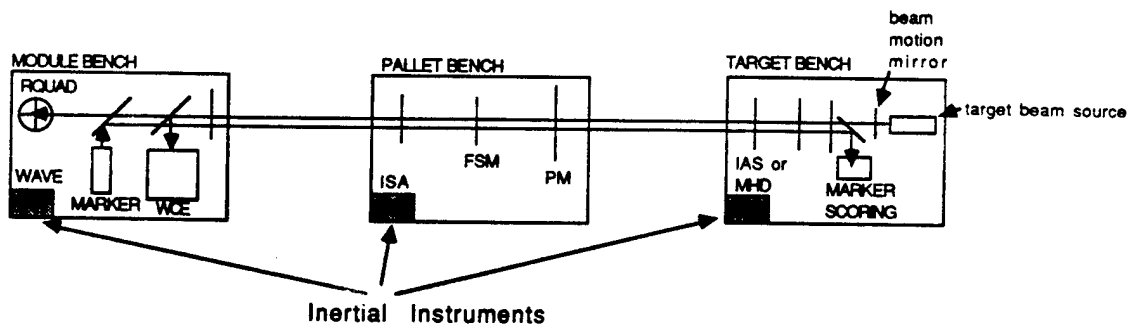
Jitter Estimate
from Coherence Analysis

Imparted Jitter

Figure 11. End-to-End Disturbance Rejection Test

14